IJCRT.ORG ISSN : 2320-2882

INTERNATIONAL JOURNAL OF CREATIVE RESEARCH THOUGHTS (IJCRT)

An International Open Access, Peer-reviewed, Refereed Journal

OPTIMIZATION OF PROCESS PARAMETERS OF WIRE ARC ADDITIVE MANUFACTURING OF 304L STAINLESS STEEL PARTS USING GREY ANALYSIS METHOD

[1]B. Mohith Kumar, [2]K. Sandeep, [3]K. Johnson, [4]M. Sai, [5]Mr. K. Sreenivasa Reddy

[1,2,3,4] Under graduate Student, [5]Assistant Professor

Department of Mechanical Engineering,

Godavari Institute of Engineering & Technology (A), 533296, Rajahmundry, AP, INDIA

Abstract: Wire arc additive manufacturing (WAAM) has emerged as a promising technique for fabricating complex geometries with metal materials. In this study, the focus is on the optimization of process parameters in WAAM of 304L stainless steel, a widely used material in various industries. Optimization of process parameters is usually aimed at improving mechanical properties and quality of the fabricated parts while minimizing defects such as porosity and distortion. In this article, we focus on predicting and optimizing process parameters for the WAAM process of 304L stainless steel. Three parameters: voltage (U), welding current (I), and travel speed (v), were considered as the input variables, and the two geometrical responses considered are width and height (WWB, HWB, respectively. Analysis of variance (ANOVA) was used to determine the impact of each input variable on the replies. The Grey-Relational Analysis (GRA) method was employed to determine the ideal process parameters. The collected results indicate that travel speed is the most significant influence on WWB and HWB. The GRA gives the exact stable process parameters, namely U = 15V, I = 75A, and v = 0.2 m/min, which were confirmed by experimental results. It was also shown that the anticipated models of WWB and HWB were suitable for choosing the process parameters in particular applications.

Keywords: WAAM, Stainless steel, Optimization, Process parameter, GRA.

I. INTRODUCTION

Wire arc additive manufacturing (WAAM) is a rapidly evolving technology that offers significant promise in the fabrication of complex metallic components with enhanced properties. Among its various applications, the production of 304L stainless steel parts through WAAM has gained substantial attention due to the alloy's widespread use in industries such as aerospace, automotive, and biomedical [1].304L stainless steel is a low-carbon variation of the 304 alloy, renowned for its excellent corrosion resistance, high-temperature strength and suitability for welding applications [2]. WAAM, as an additive manufacturing process, enables the layer-by-layer deposition of material, allowing for the creation of intricate geometries and customization of parts, which traditional manufacturing methods struggle to achieve.

Among the materials utilized in Wire Arc Additive Manufacturing (WAAM) [3], 304L stainless steel stands out as one of the most extensively studied due to its favorable weldability and high corrosion resistance. This material finds applications across diverse industries such as nuclear reactors, marine engineering, and biomedical implants. Recent research has predominantly focused on evaluating the metallurgical characteristics and mechanical properties of both thin-walled and thick-walled components fabricated using WAAM with 304L stainless steel [3]. For instance, Chen et al [4]. analyzed the microstructural characterization and tensile properties of WAAM 304L thick-walled components. Their findings revealed that

the microstructures of these components typically comprise three phases (δ, γ, and σ), with austenite γ phases being predominant, while δ and σ phases were present in small amounts within the grain boundaries of austenite. Similarly, Wang et al [5].explored the microstructural and tensile properties of WAAM 304L thick-walled parts. They focused on analyzing microstructures in the remelting zones (RZ) and overlapped zones (OZ) of weld beads in both transversal and building directions. The microstructures in RZs exhibited grains perpendicular to the fusion lines, while grains in OZs developed along the build direction, resulting in anisotropic mechanical properties. Furthermore, Wu et al [6]. investigated the fabrication of 304L stainless steel thin-walled parts using WAAM. Their observations highlighted variations in the mechanical properties of parts along the vertical direction of the thin walls. These studies collectively underscore the importance of understanding the microstructural evolution and mechanical behavior of WAAM-fabricated components using 304L stainless steel. Such insights are crucial for optimizing process parameters and ensuring the reliability and performance of components in various industrial applications.

Additional studies have looked into how processing circumstances and characteristics affect the quality of 304L steel products. The printability of multi-walled 304L components was investigated by Chakkravarthy et al [7]. using CMT-WAAM. They discovered that the surface roughness might be decreased by increasing the torch's inclination angle. The effect of heat input on the microstructure properties and corrosion of WAAM 304L components was investigated by Wen et al [8]. They noticed that while the ferrite content stayed constant, the primary dendrite spacing and corrosion resistance in microstructures rose with an increase in heat input. The inhomogeneity in the microstructures and mechanical properties of 304L stainless steel was caused by the different arc modes (such as speed pulse and speed arc) and welding-current processes (such as speed cold and speed arc) in WAAM. These findings were supported by Wu et al. and other authors. [9] Cunningham et al.'s study evaluated how LN2 cryogenic cooling affected the quality of WAAM 304L parts. The as-built components' stiffness and tensile qualities were shown to be improved by the LN2 cooling-fabricated parts, which showed more equiaxed grains than those generated under standard air-cooling conditions with an interlayer temperature of 160°C.

The prediction and optimization of processing parameters in WAAM of 304L stainless steel to get suitable geometrical features of weld beads has been the subject of very few studies up to this point. The stability of the deposition process and the ultimate shape of the products are guaranteed by the quality and shape of the individual welding beads, which include smoothness and stability as well as reduced spatter [9]. Two other crucial factors for the creation of deposition routes for the thin-walled and thick-walled components in the WAAM process are the width and height of the weld beads, denoted by WWB and HWB. For this reason, a lot of work has been done to anticipate the weld bead geometry for WAAM procedures. For example, Suryakumar et al [11]. used a parabola to simulate and validate the geometry (i.e., WWB and HWB) of weld beads in the mild steel (ER70S6) scenario. Their models have proven effective in forecasting and refining process parameters for the production of hybrid layers. Xiong et al. used an ANN (artificial neural network) and a second-order regression model to create predictive models of the WWB and HWB of low-carbon steel. They showed that their models could be utilized to estimate the desired shape of weld beads for the AM slicing process and that they had good accuracy. Wang et al [10]. They employed an ANN model to forecast the weld bead geometry for the CMT-WAAM of high-strength steel (ER100) as a function of wire feed speed, travel speed, and interpass temperature. Geng et al.[12] used the response-surface methodology (RSM) to forecast the bead shape for the GTAW-WAAM of 5A06 aluminum alloy. The effects of travel speed and wire-feed speed on WWB and HWB were examined by Youheng et al.[14]. For the bainite steel WAAM, the scientists also discovered the ideal process parameters for producing single weld beads with a smooth surface, fewer spatters, and flaws. Using RSM, Kumar and Maji. [15] created geometry models for a single weld bead in WAAM of 304L stainless steel. They then used the desirability method (DA) to improve the bead geometry. Sarathchandra. [16] and colleagues conducted study on the impact of processing factors on the geometric properties of CMT-WAAM-produced 304 stainless steel weld beads. The best process parameters were also found by using the RSM and DA methods. They demonstrated that when compared to Taguchi and RMS techniques, the TLBO showed better performance. Regressive models for the bead geometries (bead height, bead width, and symmetry coefficients) were created with a high degree of precision for the Invar alloy (nickel–iron and manganese alloy) WAAM process in the work of Veiga et al [17]. To obtain the correct weld bead form, the depositing condition could be optimized using the created models.

It is evident from the literature review above that there hasn't been much research done on how processing parameters affect the geometric properties of the weld beads in 304L stainless steel WAAM. The producers of welding wire suggested process parameters for traditional welding techniques, which were commonly followed in the production of WAAM 304L components. Our goals in this research are to anticipate the geometric properties of the weld beads and determine the ideal process parameters for the 304L steel WAAM.

Four process parameters voltage (U), welding current (I), and travel speed (v) wire feed rate (WFS) were taken into account when designing the trials using the Taguchi method and an L04 orthogonal array. The answers are provided in the following formats: width (WWB), and height (HWB) of the weld beads. The analysis of variance (ANOVA) was used to examine the significance and impact of each input variable on the replies. The GRA (Grey-Relational Analysis) method determined the ideal processing parameters[16, 17].

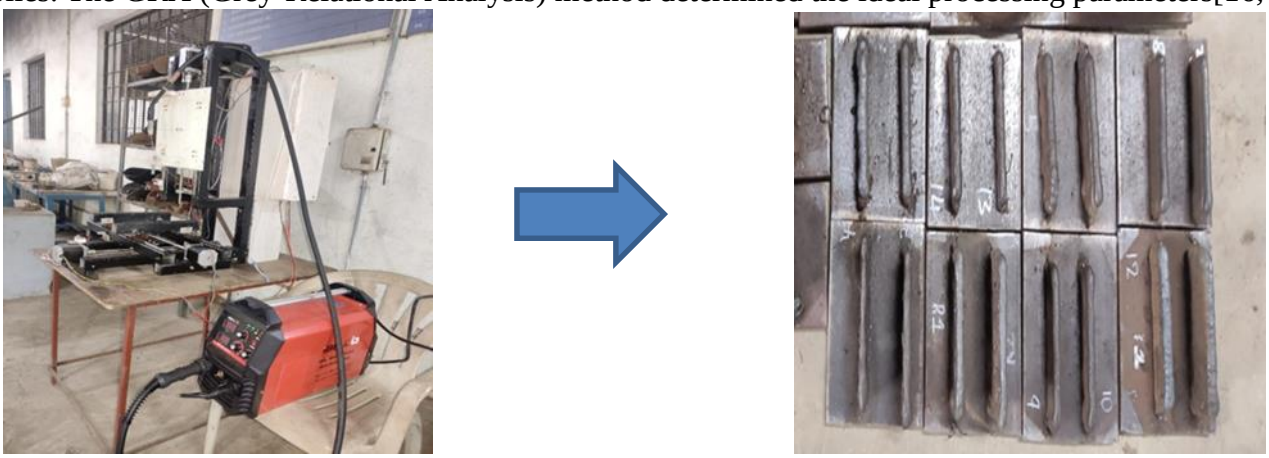

Fig. 1. WAAM of 304L Stainless Steel

II. MATERIALS AND METHODS

2.1 Materials

In the experiments, a welding wire of 304L steel with a diameter of 0.8 mm supplied by Arihant Metal was used. Two 304L-stainless-steel plates with dimensions of 100 x 80 x 10 mm were employed as the substrates. The chemical composition of the wire on the base plate is shown in Table in Table 1.

Table 1. Chemical elements of the wire and the substrate materials (in wt.%).

Element	C	Si	Mn	Ni	Cr	P
Stainless steel 304L wire	0.03	1.00	2.00	8.00	18.00	0.045
Stainless steel 304L steel	≥ 0.03	≥ 0.75	≥ 2.00	8 - 18	18 - 20	≥ 0.045

A GMAW-WAAM system, comprising a 6-axis welding robot (Panasonic TA1400) and a YD-350GR3 power, was employed to construct samples as shown in Fig. 2a. The current settings in this system are used to modify the welding wire's feed speed. As the welding process proceeds, an argon gas with to shield the molten metal from oxidation, a flow rate of 15 L/min, and a purity of 99.99% were used.

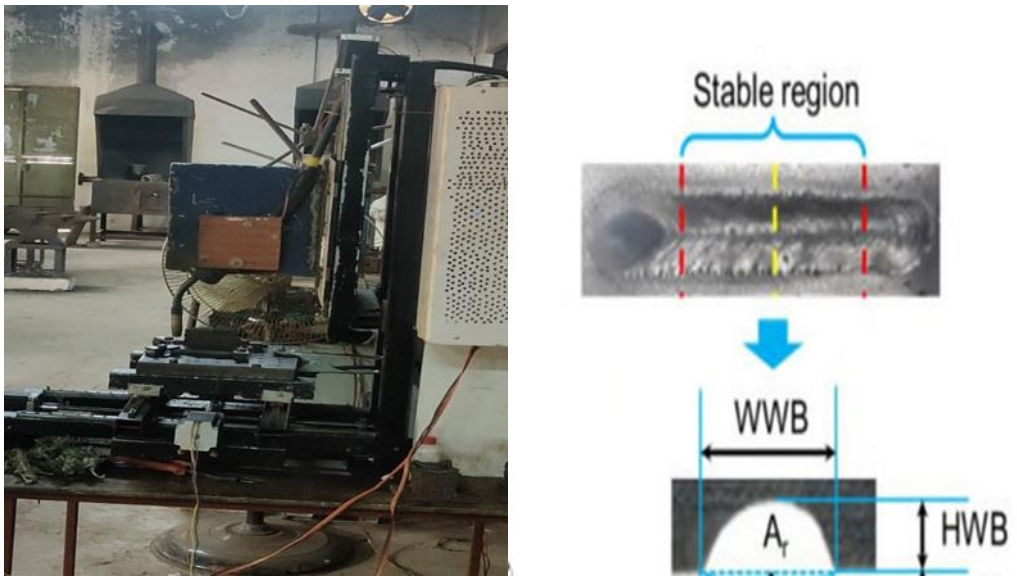

Fig. 2. (a) the WAAM system, (b) a single weld bead, and (c) a cross-section image of WWB and HWB.

2.2 Research Procedure

As previously indicated, the main goals of this work are to identify the ideal processing parameters in the WAAM of 304L stainless steel and to evaluate the impact of input parameters {I, U, v} on the geometrical properties of single weld beads {WWB and HWB}. To fulfill these goals, the proposed research methodology is depicted in fig. 3. The following is a diagram of the main steps:

2.2.1 Determining the limited values of the input variables

Every input variable's limited values that is, its lowest and greatest values were established. To do that, we did several trials using single weld beads and process parameter values that were within the ranges suggested by the wire provider for traditional welding procedures. Following a few trial runs, the following value ranges for travel speed, voltage, and welding current were established: The values of I = 75–104 A, U = 15–23 V, and v = 0.2–0.35 m/min enable the production of continuous weld beads with fewer spatters, as seen in Figure 2b).

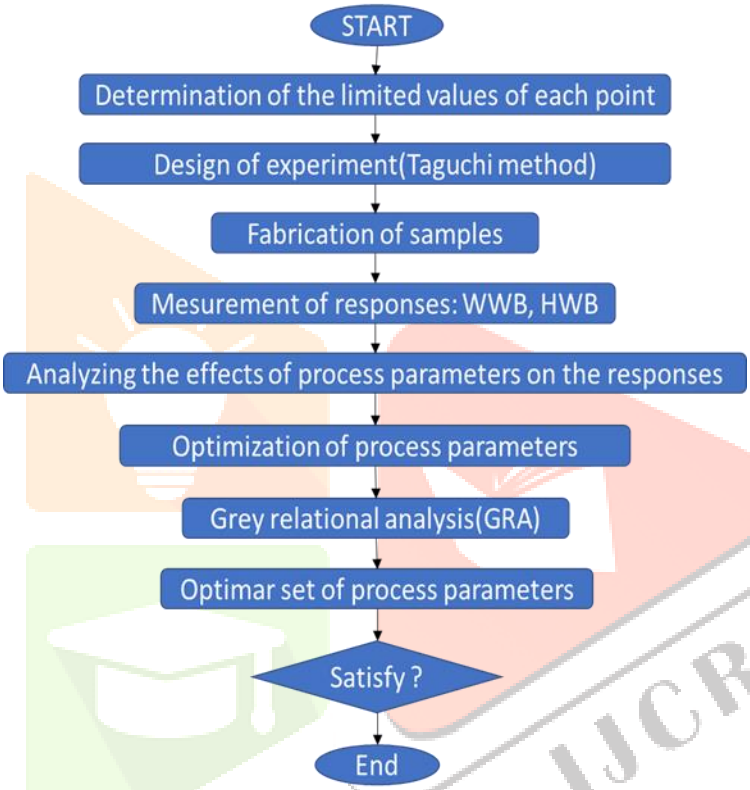

Fig. 3. Research methodology

2.2.2 Data collection and experiment design

The tests were designed by the L16 orthogonal array and the Taguchi method. In contrast to other approaches to experimental design, including full factorial design and RSM, the Taguchi technique allows for the simultaneous optimization of several parameters and the extraction of more quantitative data from fewer experimental runs. As a result, the Taguchi experimental design can offer reliable design solutions, lower costs, and enhance quality. Three input variables with four levels were chosen for this investigation, as shown in Table 2. 16 experimental runs of single weld beads were therefore conducted to gather data on the responses that were taken into consideration (i.e., WWB and HWB). The GMAW-WAAM system mentioned above produced each weld bead, which had a length of roughly 60 mm, on two surfaces. The substrate was cooled to room temperature for the subsequent runs following each run. Therefore, we presumed that the prior weld bead run had no impact on the subsequent weld beads' geometrical reactions. Table 3 displays the experimental design and measurement outcomes.

The average values of five measurements at five different sites within a stable zone of weld beads were used to determine the values of WWB and HWB (Fig. 2). Using a digital Mitutoyo caliper with a resolution of 0.01 mm and an accuracy of ± 0.02 mm, the WWB and HWB at a position were measured.

Table 2. Process parameters and their levels were used for the design of the experiment.

Process parameter	Levels			
	1	2	3	4
I(A)	75	85	94	104
U(V)	15	20	21.5	23
V(m/min)	0.2	0.25	0.3	0.35

Table 3. Experimental plan and the measurement results of responses.

I	U	V	WWB	HWB
75	15	0.2	6.5	3.8
75	20	0.25	8.7	3.2
75	21.5	0.3	8.1	2.2
75	23	0.35	8.2	1.9
85	15	0.25	6.8	3.8
85	20	0.2	8.7	3.4
85	21.5	0.35	8.5	2.6
85	23	0.3	9.7	2.2
94	15	0.3	6.2	3.8
94	20	0.35	7.7	3.0
94	21.5	0.2	10.5	3.6
94	23	0.25	10.6	2.5
104	15	0.35	6.5	3.1
104	20	0.3	8.2	2.9
104	21.5	0.25	9.6	2.8
104	23	0.2	11.2	3.5

2.2.3 Analysis of the impacts of processing parameters on the responses

ANOVA (analysis of variance), the impact of process factors on the responses was assessed. A 95% confidence level was used to conduct the ANOVA and the prediction models for each response by utilizing Minitab for software.

2.2.3 Optimization of processing parameters

GRA (Grey-Relational Analysis) method was used in this work to solve the multi-response optimization problems. These techniques are successfully used in various production domains, such as welding and machining. The following is the definition of the multi-response optimization problem of weld beads in the WAAM process:

Find X = {U, I, V} that

Subject to 75≤ I ≤ 104 A, 15 ≤ U ≤ 23 V, and 0.2 ≤ V ≤ 0.35 m/min.

2.3 Grey Relational Analysis (GRA)

Normalizing the responses is the first stage in the GRA approach. The large-the-better (LTB) and smaller-the-better (STB) are two types of quality characteristics. The WWB and HWB variables in this instance were standardized using LTB, Eq. (1):

$$y_{ij}^{(n)} = \frac{y_{ij}^{(0)} - Min\left\{y_{ij}^{(0)}\right\}}{Max_i\left\{y_{ij}^{(0)}\right\} - Min_i\left\{y_{ij}^{(0)}\right\}} \quad , \text{I} = 1,2,\ldots, \text{m and j} = 1,2,\ldots,\text{n} \qquad (1)$$

Whre $y_{ij}^{(0)}$is the initial reaction that the experiments measure, $Max_i\left\{y_{ij}^{(0)}\right\}$is the maximum value of $\left\{y_{ij}^{(0)}\right\}, Max\left\{y_{ij}^{(0)}\right\}$ is the minimum value of $\left\{y_{ij}^{(0)}\right\}$, "m" is the number of experimental runs, and "n" is the number of responses.

In the second step, the grey relational coefficient (GRC) was computed by Eq. (2):

$$\epsilon_{ij} = \frac{\delta_{min}+\omega_{max}}{\delta_{0i}(k)+\omega\delta_{max}} \quad (2)$$

Where δ_{0ij} is the absolute deviation between the comparability $y_{ij}^{(n)}$ and the reference $y_{0j}^{(n)}$, as described in Eq. (3); δ_{max} and δ_{min} are the maximum and minimum values of $\delta_{0i}(k)$, as shown in Eqs. (4) and (5), respectively; and ω is a distinguishing coeff omega is Generally, the value of ω is set to 0.5.

$$\delta_{0ij} = \left|y_{ij}^{(n)} - y_{0j}^{(n)}\right| \quad (3)$$

$$\delta_{min} = min_{\forall i}\{min_{\forall j}\delta_{0ij}\} \quad (4)$$

$$\delta_{max} = max_{\forall i}\{max_{\forall j}\delta_{0ij}\} \quad (5)$$

Lastly, using Eq. (6), the gray relational grade was determined.

$$\aleph_i = \sum_{j=1}^{n} w_i * \epsilon_{ij} \quad (6)$$

Where w_i refers to the weight of the i^th objective and $\sum_{i=1}^{n} w_i = 1$. The value of $\aleph_i$ falls in the range from 0 to 1, and the optimal solution is corresponding to the highest value of $\aleph_i$.

III RESULTS AND DISCUSSION

3.1. Impact of process parameters on the results

3.1.1. Parameters effects on the width of welding beads (WWB)

Figure 4 illustrates how process parameters directly affect WWB. It is discovered that an increase in welding voltage (from 15 to 23 V) and current (from 75 to 104 A) results in an increase in WWB.

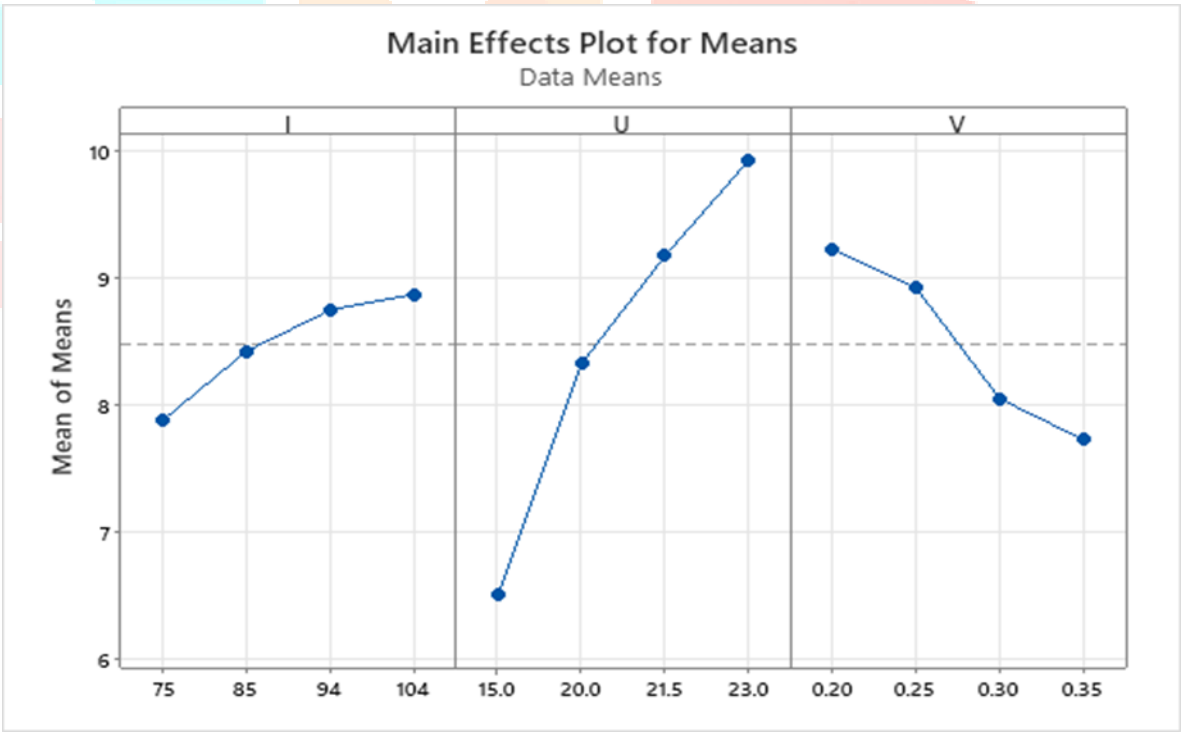

Fig. 4. Direct effects of process parameters on WWB

However, a decrease in WWB results from increasing the travel speed (from 0.2 to 0.35 m/min). Process parameters' effect on the answers.

These events can be explained by the following arguments, the size of the melting pool and the width of the weld beads (WWB) rise as a result of an increase in welding current, which also causes an increase in wire feed speed and material deposition. Additionally, there is a voltage increase makes the arc longer and more widely spaced. As a result, WWB grows as the voltage level increases. On the other hand, a rise in travel speed causes the amount of material deposited per unit of length to decrease. As a result, as travel speed rises, the WWB gets narrower.

The outcome of the ANOVA on the importance of each parameter for WWB are displayed in Table 4. The data suggests that travel speed has the greatest impact on WWB, accounting for 49.36% of the total contribution. Voltage comes in second with 41.75% of the contribution. The welding current, on the other hand, has the least impact only 4.43% of the total contribution percentage. The WWB projected model is shown in Eq. (6). According to the determination coefficients, which are greater than 90% respectively, this model may be utilized for prediction and has a high accuracy.

$$WWB(mm) = -0.02 + 0.03447\ I + 0.4215\ U - 10.78\ V$$

Table 4. ANNOVA for WWB

Source	DF	Adj SS	Adj MS	F-value	P-value
Regression	3	33.720	11.2401	75.55	0.000
I	1	2.191	2.1908	14.73	0.002
U	1	25.719	25.7190	172.88	0.000
V	1	5.810	5.8104	39.06	0.000
Error	12	1.785	0.1488		
Total	15	35.505			

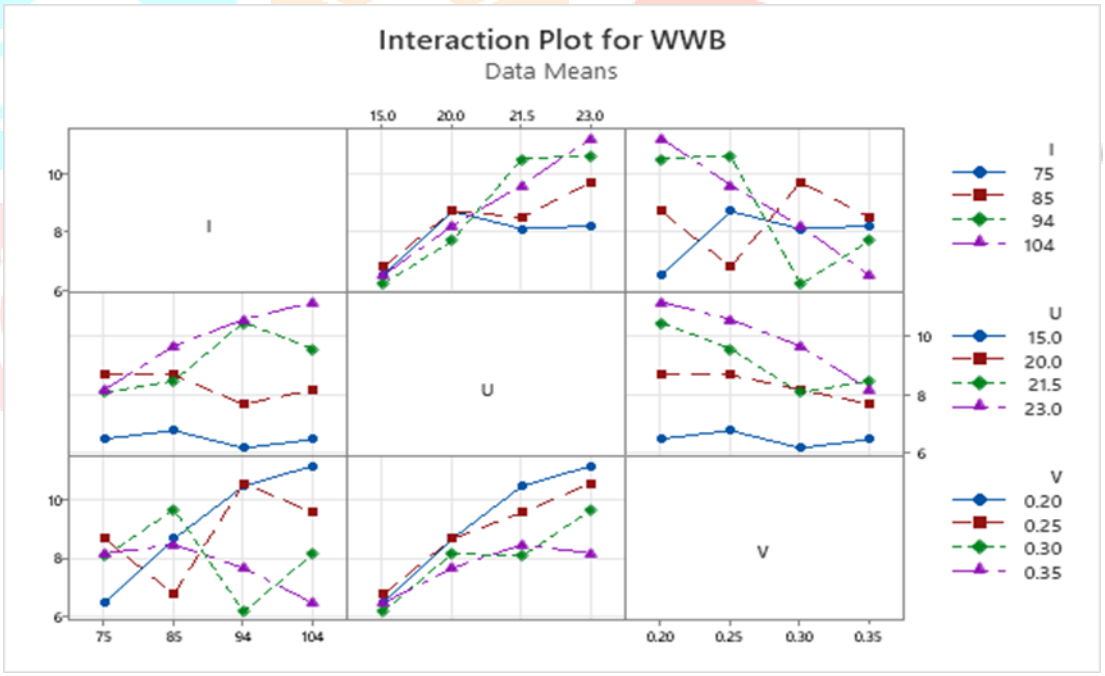

Fig. 5. Interaction effects of process parameters on WWB

The cumulative effects of process factors on WWB are shown in Figure 5. The WWB typically rises or falls as the voltage and welding speed increase, respectively, in the design space of because of the significant contribution percentages of travel speed and voltage on WWB. trials. In the meantime, only in situations involving high voltages and moderate travel speeds does the WWB rise in tandem with an increase in welding current. In cases when the travel speed is fast (0.35 m/min) or the voltage is low (e.g., 15V), the WWB exhibits a declining pattern as the welding current increases.

3.1.2. The impact of parameters on the weld beads' height (HWB)

Fig. 5 describes the primary effects of process factors on the HWB. It is discovered that when welding current increases from 75 to 104 A, the HWB rises as well. Conversely, HWB declines as either the travel speed rises from 0.2 to 0.35 m/min, or the voltage rises from 15 to 23 V. As was previously mentioned, the wire feed speed increases in tandem with the welding current. Consequently, there is an increase in the

volume of materials deposited, which raises HWB[15]. Additionally, as the welding current rises, the convexity of the weld beads rises as well. This improves the HWB as well.However, the amount of materials deposited per unit of length decreases with an increase in travel speed. As a result, the HWB is decreased [15]. Flatter weld beads result from a greater arc spreading area caused by an increase in voltage [17]. Consequently, the HWB has a declining tendency with an voltage rise.

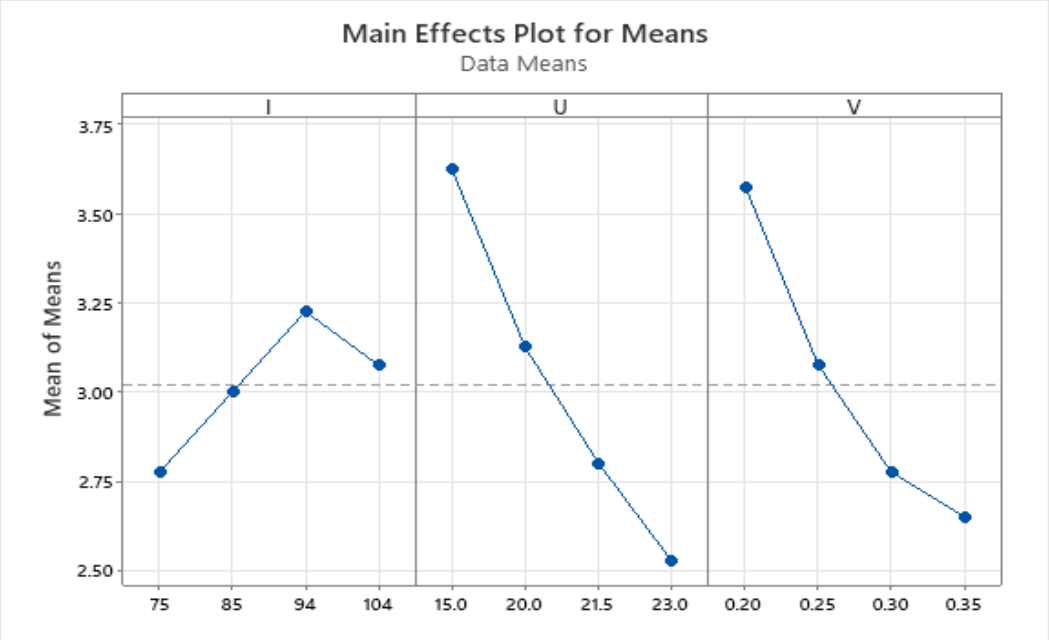

Fig. 6. Direct effects of process parameters on HWB

The HWB ANOVA findings are displayed in Table 5. With a 54.34% contribution, the travel speed is determined to have the greatest effect on HWB. The impact contribution is displayed by the voltage at 24.03% and the welding current at 14.78%, respectively. These outcomes also line up with the data displayed in Figure 5 shows that the HWB model that was constructed is likewise suitable for the prediction with a respectable level of accuracy greater than 90%.

$$HWB(mm) = 6.327 + 0.01163\ I - 0.1338\ U - 6.15\ V$$

Table 5. ANNOVA for HWB

Analysis of Variance (HWB)

Source	DF	Adj SS	Adj MS	F-value	P-value
Regression	3	4.7307	1.57689	19.84	0.000
I	1	0.2495	0.24951	3.14	0.102
U	1	2.5900	2.59003	32.59	0.000
V	1	1.8911	1.89113	23.79	0.000
Error	12	0.9537	0.07948		
Total	15	5.6844			

Fig. 6 illustrates how input parameter interactions affect the HWB. Similar to the situation of WWB, the HWB often decreases over the whole experiment's design space as the moving speed rises. According to Table 5, this suggests that the travel speed has the greatest effect on the HWB. The Additionally, a declining tendency with an increase in voltage is revealed by 15 HWB. However, the HWB exhibits an increasing tendency with an increase in voltage at high current levels (I = 104 A) and low travel speeds (v = 0.2 m/min). However, the welding current shows a complicated interplay with other HWB parameters.

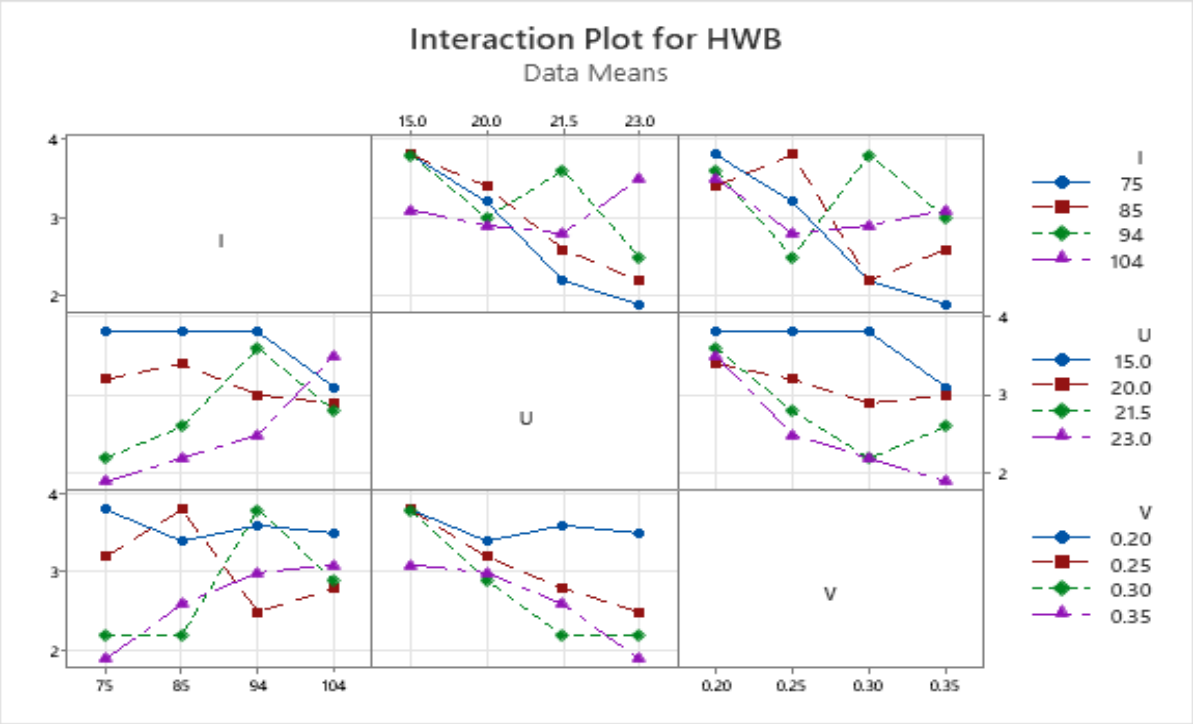

Fig. 7. Interaction effects of process parameters on HWB.

3.2. Optimization results

3.2.1. Optimization with GRA

Table 6 shows the results of the computation using the GRA approach. For WWB and HWB, the normalized responses were derived using Eq. (1) was used to generate the GRC values, and Eq. (6) was then used to obtain the GRG values. It should be noted that the CRITIC approach was used to determine the weight for each response in Eq. (6). The WWB and HWB weights in this study are required respectively. The rank for each alternative is shown in Table 7's final column based on the GRG values. The ideal condition is defined as Run 1 having the highest GRG value. The best combination of process parameters is therefore the set of parameters associated with Run 1. Table 8 displays the average values of GRG for each level of input variable.

The optimal conditions with the largest GRG are also shown in Fig. 11 and are indicated by bolded numerals. The optimal process parameters are U = 15 V, I = 75 A, and v = 0.2 m/min. According to the ANOVA for GRG, the welding current has a negligible impact (P-value > 0.05) with just 0.10% of contribution, however the voltage and welding speed have substantial affects on GRG (P-value < 0.05) with 51.49% and 16.91% of contribution, respectively.

Table 6. Calculation results of normalized responses, GRC, GRG, and ranking.

Run	Normalized Response		Grey Relational Coefficient		GRG	Rank
	WWB	HWB	WWB	HWB		
1	0.06	1	0.347222222	1	3.680555556	1
2	0.5	0.684210526	0.5	0.612903226	2.985919099	6
3	0.38	0.157894737	0.446428571	0.37254902	2.799929972	9
4	0.4	0	0.454545455	0.333333333	3.121212121	5
5	0.12	1	0.362318841	1	3.382727004	2
6	0.5	0.789473684	0.5	0.703703704	2.573318216	12
7	0.46	0.368421053	0.480769231	0.441860465	2.895418812	7
8	0.7	0.157894737	0.625	0.37254902	2.522719088	13
9	0	1	0.333333333	1	3.366169154	3
10	0.3	0.578947368	0.416666667	0.542857143	2.836804075	8
11	0.86	0.894736842	0.78125	0.826086957	2.754458492	11

12	0.88	0.315789474	0.806451613	0.422222222	2.423414418	14
13	0.06	0.631578947	0.347222222	0.575757576	3.256313131	4
14	0.4	0.526315789	0.454545455	0.513513514	2.345836746	15
15	0.68	0.473684211	0.609756098	0.487179487	2.239792728	16
16	1	0.842105263	1	0.76	2.76	10

Table 7. Average values of GRG according to the input variables levels.

Level	I(A)	U(V)	V(mm/min)
1	3.146	2.421	2.942
2	2.843	2.513	2.757
3	2.845	2.672	5.517
4	10.601	2.706	3.027
Delta = Max - Min	7.758	0.908	2.575
Rank	1	3	2

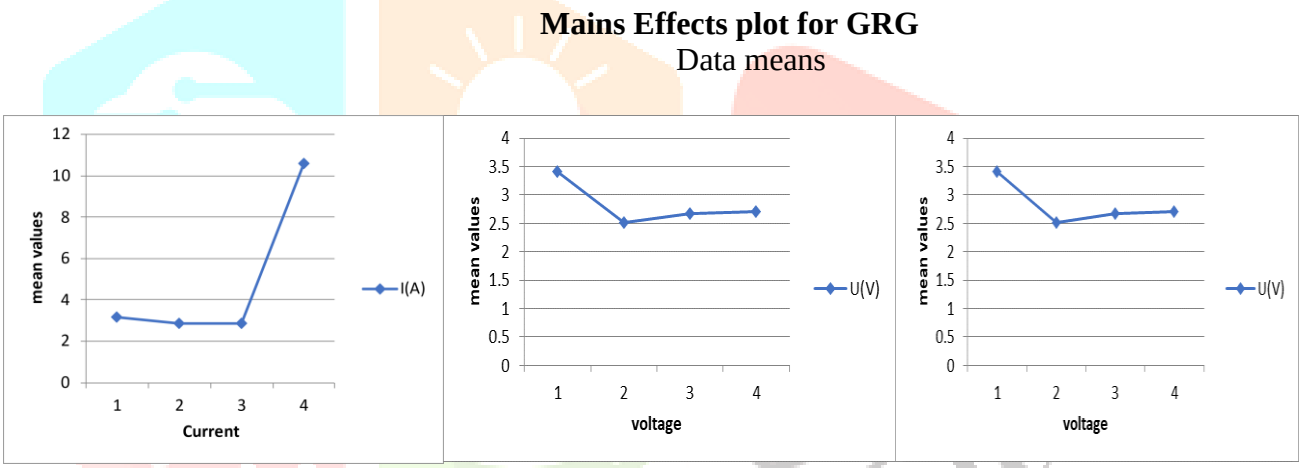

Fig. 8. Effects of process parameters on GRG

From the obtained results, it is observed that the GRA method recommends a similar set of optimal process parameters. Therefore, we can conclude that the optimal process parameters for the WAAM process of 304L stainless steel according to the defined optimal criteria are I= 75 A, U = 15 V, and v = 0.2 m/min.

To validate the optimal process parameters, these parameters have been used to build a cylinder wall with 20 layers of single beads, as shown in Fig. 9. It is revealed that the single weld bead is 24 continuous and smooth with a regular width (Fig.9).The parallel of a line wall also has a good shape and regular height and width (Fig. 9).

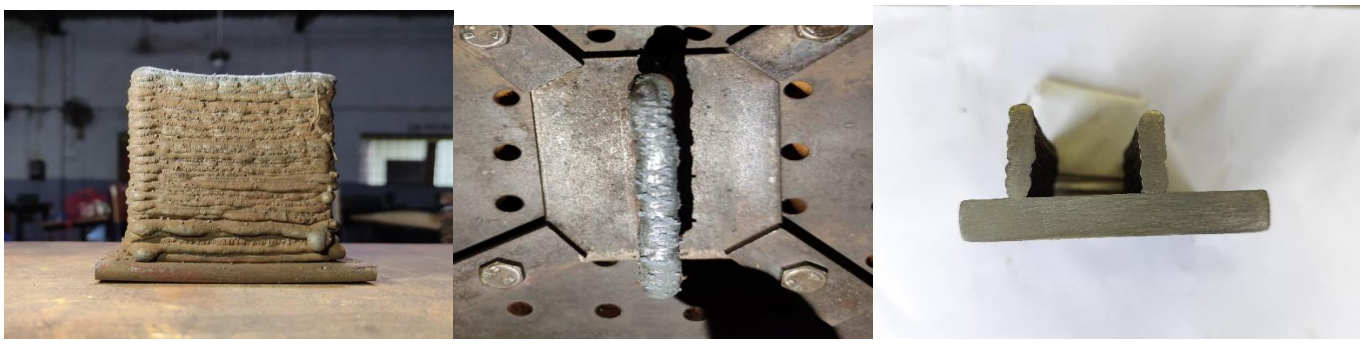

Fig. 9. Single weld bead and 20-layer Single wall Structure produced by the WAAM process with the optimal process parameters.

IV CONCLUSION

The purpose of this study was to determine how the GMAW-WAAM process of 304L stainless steel, which includes the width and height of weld beads (WWB and HWB), was affected by process factors. Using L16 in the Taguchi technique, an orthogonal array was used in the experiment design. To determine the impact of input variables on each response, an ANOVA was used. The GRA methodology was also used to identify the ideal process parameters. The primary findings of this study can be summarized as follows:

- The properties of individual weld beads are significantly influenced by the process conditions. According to the ANOVA results, the travel speed has the biggest impact on the WWB and HWB.
- When it comes to forecasting the process parameters in particular applications, such as generating deposition routes, slicing layers from 3D CAD models for AM, and thermo-mechanical simulations of the WAAM process, the models of WWB and HWB are also sufficient. The primary method for handling multi-objective decision-making issues is GRA.
- The same ideal process parameters for 304L stainless steel in WAAM are provided by GRA method: U = 15 V, I = 75 A, and v = 0.2 m/min. These values were successfully employed to construct 20 layers that were deposited on the Single wall. The constructed part's stable and regular geometry proves that the ideal process parameters were used.

REFERENCES

[1] D. Jafari, T. H. J. Vaneker, and I. Gibson, "Wire and arc additive manufacturing: Opportunities and challenges to control the quality and accuracy of manufactured parts," *Mater. Des.*, vol. 202, p. 109471, Apr. 2021, doi: 10.1016/j.matdes.2021.109471.

[2] S. Pattanayak and S. K. Sahoo, "Gas metal arc welding based additive manufacturing—a review," *CIRP J. Manuf. Sci. Technol.*, vol. 33, pp. 398–442, May 2021, doi: 10.1016/j.cirpj.2021.04.010.

[3] V. T. Le, D. S. Mai, and Q. H. Hoang, "A study on wire and arc additive manufacturing of low-carbon steel components: process stability, microstructural and mechanical properties," *J. Braz. Soc. Mech. Sci. Eng.*, vol. 42, no. 9, p. 480, Sep. 2020, doi: 10.1007/s40430-020-02567-0.

[4] X. Chen, J. Li, X. Cheng, B. He, H. Wang, and Z. Huang, "Microstructure and mechanical properties of the austenitic stainless steel 316L fabricated by gas metal arc additive manufacturing," *Mater. Sci. Eng. A*, vol. 703, pp. 567–577, Aug. 2017, doi: 10.1016/j.msea.2017.05.024.

[5] C. Wang, T. G. Liu, P. Zhu, Y. H. Lu, and T. Shoji, "Study on microstructure and tensile properties of 316L stainless steel fabricated by CMT wire and arc additive manufacturing," *Mater. Sci. Eng. A*, vol. 796, p. 140006, Oct. 2020, doi: 10.1016/j.msea.2020.140006.

[6] W. Wu, J. Xue, L. Wang, Z. Zhang, Y. Hu, and C. Dong, "Forming Process, Microstructure, and Mechanical Properties of Thin-Walled 316L Stainless Steel Using Speed-Cold-Welding Additive Manufacturing," *Metals*, vol. 9, no. 1, p. 109, Jan. 2019, doi: 10.3390/met9010109.

[7] V. Chakkravarthy and S. Jerome, "Printability of multiwalled SS 316L by wire arc additive manufacturing route with tunable texture," *Mater. Lett.*, vol. 260, p. 126981, Feb. 2020, doi: 10.1016/j.matlet.2019.126981.

[8] D. Wen, P. Long, J. Li, L. Huang, and Z. Zheng, "Effects of linear heat input on microstructure and corrosion behavior of an austenitic stainless steel processed by wire arc additive manufacturing," *Vacuum*, vol. 173, p. 109131, Mar. 2020, doi: 10.1016/j.vacuum.2019.109131.

[9] C. R. Cunningham, V. Dhokia, A. Shokrani, and S. T. Newman, "Effects of in-process LN2 cooling on the microstructure and mechanical properties of type 316L stainless steel produced by wire arc directed energy deposition," *Mater. Lett.*, vol. 282, p. 128707, Jan. 2021, doi: 10.1016/j.matlet.2020.128707.

[10] Z. Wang, S. Zimmer-Chevret, F. Léonard, and G. Abba, "Prediction of bead geometry with consideration of interlayer temperature effect for CMT-based wire-arc additive manufacturing," *Weld. World*, vol. 65, no. 12, pp. 2255–2266, Dec. 2021, doi: 10.1007/s40194-021-01192-2.

[11] H. Geng, J. Xiong, D. Huang, X. Lin, and J. Li, "A prediction model of layer geometrical size in wire and arc additive manufacture using response surface methodology," *Int. J. Adv. Manuf. Technol.*, vol. 93, no. 1–4, pp. 175–186, Oct. 2017, doi: 10.1007/s00170-015-8147-2.

[12] S. Suryakumar, K. P. Karunakaran, A. Bernard, U. Chandrasekhar, N. Raghavender, and D. Sharma, "Weld bead modeling and process optimization in Hybrid Layered Manufacturing," *Comput.-Aided Des.*, vol. 43, no. 4, pp. 331–344, Apr. 2011, doi: 10.1016/j.cad.2011.01.006.

[13] F. Youheng, W. Guilan, Z. Haiou, and L. Liye, "Optimization of surface appearance for wire and arc additive manufacturing of Bainite steel," *Int. J. Adv. Manuf. Technol.*, vol. 91, no. 1–4, pp. 301–313, Jul. 2017, doi: 10.1007/s00170-016-9621-1.

[14] A. Kumar and K. Maji, "Selection of Process Parameters for Near-Net Shape Deposition in Wire Arc Additive Manufacturing by Genetic Algorithm," *J. Mater. Eng. Perform.*, vol. 29, no. 5, pp. 3334–3352, May 2020, doi: 10.1007/s11665-020-04847-1.

[15] D. T. Sarathchandra, M. J. Davidson, and G. Visvanathan, "Parameters effect on SS304 beads deposited by wire arc additive manufacturing," *Mater. Manuf. Process.*, vol. 35, no. 7, pp. 852–858, May 2020, doi: 10.1080/10426914.2020.1743852.

[16] K. Venkatarao, "The use of teaching-learning based optimization technique for optimizing weld bead geometry as well as power consumption in additive manufacturing," *J. Clean. Prod.*, vol. 279, p. 123891, Jan. 2021, doi: 10.1016/j.jclepro.2020.123891.

[17] F. Veiga, A. Suarez, E. Aldalur, and T. Artaza, "Wire arc additive manufacturing of invar parts: Bead geometry and melt pool monitoring," *Measurement*, vol. 189, p. 110452, Feb. 2022, doi: 10.1016/j.measurement.2021.110452.